Energy Transfer Strategies in Magnetic Resonance Based Intrabody Networks

Hirsa Kia, Pramita Pandit, Krishna Kant
Temple University

***Abstract*—In this paper we explore strategies for providing energy to nodes of *small* intrabody networks of sensors, actuators, and decision support nodes that are deployed to manage chronic illnesses. In particular, we study both a centralized and decentralized mechanism for energy transfer by using magnetic resonance communication (MRC), which is suitable for through-the-body communications up to a meter distance. We demonstrate that while the centralized mechanism can maintain a higher energy level for the critical "hub" nodes of the network, and decentralized mechanism not only has a lower overhead but is also more robust and can deal with adverse events (e.g., energy starvation) better. We also explore a hybrid strategy in order to harness the advantages of both centralized and decentralized schemes.**

***Index Terms*—intra-body network, Magnetic resonance communication, Power distribution.**

I. Introduction

Chronic diseases are on a rapid rise throughout the world due to the rapidly aging population in developed countries and the increase in air, water, and food pollution in developing countries [1], [2]. According to the US CDC, *chronic* diseases account for nearly 75% of aggregate healthcare spending, and their treatment accounts for 96% of Medicare and 83% of Medicaid costs [3], [4]. Since the likelihood of multiple chronic conditions increases with age [5], the rapidly growing geriatric population argues for *small* networks of sensors, actuators, and possibly controllers to manage the chronic illnesses.

For example, overactive bladder control may involve sensors to measure bladder pressure, urine volume, EMG signal, etc. [6]–[9]. Similarly, personalized management of diabetes could benefit from measurements of gastrointestinal parameters (e.g., pH, insulin, enzymes, etc.). An effective pacemaker control benefits from oxygen, respiration, activity, and other measurements [10], [11]. The intervention (or actuation) could itself be manual (e.g., operation of an insulin pump) or automated (e.g., neuro-modulation for overactive bladder control) depending on the specific chronic condition and the signals required.

In general, the network node may either be implanted or worn on-body. Drug injectors (e.g., an insulin pump) are likely to best installed on-body, whereas sensors may be more convenient if implanted. In any case, we need a through-the-body communication mechanism for which we use *Magnetic Resonance Communications* (MRC) for reasons described later in the paper. The resulting Chronic Disease Management Network (CDMN) must operate efficiently and reliably for long periods, ideally the lifetime of the patient. Integrating a life-time battery with every node is largely impractical because batteries are often the largest part of an implanted node, may still not last the lifetime, and could pose toxicity challenges. Instead, we assume that each node carries a small supercapacitor that is charged via wireless power transfer (WPT), again using MRC. We assume that the energy is supplied by an on-body node (OBN) such as a smartwatch or stomach patch, although in-body energy harvesting may also be possible close to moving parts like the heart, lung, etc. [12], [13]. In any case, the overall mechanism requires an integrated energy transfer and communications mechanism. In this paper, we focus on WPT only; some of the basic communications issues are explored in [**?**] and others are being explored in our ongoing work [14].

It is important to note at the outset that *practical intrabody networks are likely to be very small in size and thus their scalability is not a significant concern.* The key reason is that every implanted node requires an invasive surgical procedure and risks of potential harm and malfunction. Even the wearable nodes for medical purposes are expected to be rather few because of user inconvenience. Thus, the primary focus of such networks is *not* scalability, but rather simplicity, energy efficiency, and ability to cope with energy deficiency scenarios.

In this paper, we explore energy transfer strategies to an entirely intra-body CDMN from an OBN such as a smartwatch. We compare two mechanisms in this regard: a *centralized* mechanism where the OBN maintains the energy status of all the nodes, and a *decentralized* mechanism where each node determines the energy needs for itself. The main contributions of the paper are as follows:

1) We build a detailed energy-centric simulation model of CDMN that accounts for all key components of energy supply, storage, and consumption, and calibrate it using the best available/estimated parameters for the body media.
2) We evaluate the energy level of each node in CDMN under the centralized and decentralized mechanisms under both normal and unreliable energy supply scenarios.
3) We demonstrate that while the centralized scheme achieves better performance than the decentralized scheme, it is rather sensitive to the parameters. We also show that a hybrid strategy that combines centralized and decentralized schemes can provide the advantages of both.

WPT through the body has been explored extensively, but to the best of our knowledge, the literature only speaks of WPT to

This research was supported by NSF grant CNS-2245088

a single node rather than a network. For example, NFMI [9], [15], [16], ultrasound [17] and comparison between various techniques [18], [19]. Impedence matching and frequency drift in NFMI has also been studied [20], [21]. Although these works optimize point-to-point energy delivery, they do not offer any strategies for coordinating energy across a network of nodes. Also, nearly all the work on energy transfer through the human/animal tissue media is focused on very short distances, at most a few cm, but largely in the mm range.

In this paper, we focus on powering the CDMN nodes by transferring energy from a battery-operated OBN rather than via on-body or in-body energy harvesting. Energy harvesting in the body has been explored extensively both in terms of technologies such as piezoelectric (from movements), thermoelectric, tribo-electric, etc [22]. Of these, only piezoelectric can reach 1mW or higher level, which is essential to power sensors more than a few cm away. However, piezoelectric powering would need sustained movements above some threshold, but only the heart/lungs can be considered as reliable, yet can generate only a few hundreds of μW of power [23]. While arms/legs can generate a substantial amount of energy, the movements are at best erratic (almost absent during sleep/sickness, in disabled people, etc.). Even in scenarios where milli-Watt-level power can be harvested, the challenge of efficiently transmitting this energy to distant nodes needs to be addressed.

While not directly comparable, there are some computationally intensive solutions in large-scale wireless networks operating in air media that use bio-inspired heuristics and deep reinforcement learning to select one recipient node per round or determine power allocation among users [24], [25]. However, extending such methods to support multiple recipients would drastically increase complexity due to the combinatorial search space and path evaluations, making them impractical for small, real-time networks like CDMN.

II. Chronic Disease Management Networks

A. Communications and Energy Transfer Through the Body

Although there are several suitable technologies for through-the-body wireless communications (TBWC), we focus here only on Magnetic Resonance Communication (MRC), which uses a resonant pair of transmitter and receiver. An MRC antenna has a coil in parallel with a capacitor, thereby forming an LC circuit. Such a circuit has a natural resonance frequency given by $1/(2\pi\sqrt{LC})$, traditionally chosen to be 13.56 MHz (RFID frequency), although the optimal frequency for intra-body use is around 25-30MHz [26]. The low-frequency results in nonradiative energy transfer, primarily through magnetic induction between the two coils. A precise matching of the resonance frequency and impedance on the transmit and receive side results in efficient energy transfer, and an autotuning mechanism can be used to ensure retaining high gain despite the disturbances [27].

MRC has been evaluated both experimentally and via detailed human body simulations [26], [28], [29], and it is found that the technology shows only a small person-to-person variation and is very robust against movements, posture changes, clothing, etc. The MRC attenuation through the body varies from 15 to 23db in the body-length range, which makes the technology quite suitable for intrabody communications. However, a $\sim$20 db signal loss is quite steep for WPT; it means that if we send 1mW, only 10μW of it will reach the receiver. This emphasizes the need to make the WPT as efficient as possible.

B. Organization of CDMN

Fig. 1 illustrates the network architecture, shown with a single *on-body node* (OBN) worn on the wrist using a smartwatch-like device with a special antenna attachment at the bottom to contact the skin. The OBN serves a crucial function of supplying energy to in-body nodes in addition to being an overall controller of the system with both local computing/display capabilities and the ability to connect to more powerful external devices via WiFi or BlueTooth. OBN does bring in security issues for which one may use standard tools like (hardware) trusted computing, lightweight cryptography, and a trust-but-verify approach by internal nodes for external interactions; however, tackling security or its energy implications is beyond the scope of this paper.

Fig. 1 shows a CDMN composed of multiple clusters, one for each chronic disease, where each cluster has a "hub" for data gathering from its sensors (expected to be located nearby) and making disease-specific alerting/actuation decisions. The OBN would thus interact only with the hub nodes, which in turn interact with the sensors for data transfer and configuration. The figure also shows optional in-body (energy) harvesting nodes (IBHNs) to power the hubs.

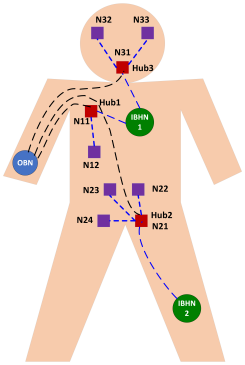

Fig. 1: A Sample CDMN

C. Energy Transfer from OBN to Intrabody Nodes

The human body is an extremely complex media for electromagnetic energy because the key properties of various organs (i.e., electrical permittivity and conductivity) vary over a very wide range. Thus, the signal attenuation from transmitter to receiver is very different than through the air. In particular, a simple application of Lenz's law for near-field magnetic induction would suggest a received power decay as $1/d^6$ and high directionality (i.e., signal strength decays as the cosine of the angle from the perpendicular to the center of the flat coil antenna) [30]. Neither is true for the body media. The signal decays far more slowly, likely due to the significant conductivity of the body. Also, the relative orientation of transmit and receive coils does not matter much, likely due to highly heterogeneous media that will cause substantial reflection/diffraction of the signal at each interface of organs with different permittivities [29].

On the plus side, this implies that the antennas do not need to be oriented precisely, which is rather difficult because of the constant movement of muscles and other body organs hosting the implanted nodes. On the negative side, this means that the signal, particularly in the context of energy transfer, cannot be directed toward a specific node that is low on energy and needs to be charged. Thus, every intrabody node can attempt to receive the energy whenever it is being supplied by the OBN. Section IV-A discusses our real (on-body) experiments to explore the impact of multiple receivers receiving the signal simultaneously. We find that this decreases the amount of energy available to each node, but the total energy received is approximately the same. The energy received by any given node depends on their distance from OBN and precise locations in the body. Thus, we need to decide which nodes will receive the energy depending on many factors, including their locations, energy needs, number of simultaneous receivers, etc. We design both a centralized anda decentralized algorithm to dynamically determine the receivers.

III. Integrated Communication and Energy Transfer

A. Communications Scheduling

The CDMN considered here is naturally quite small in size. Also, the implanted sensor nodes would typically generate a very small amount of data for each sample – perhaps only a few 10's bytes, even if monitoring multiple quantities.[1] These aspects, coupled with the need for high energy efficiency, suggest a simple scheduled media-access layer (MAC) for CDMN. That is, every message type will be assigned a specific time-slot so that it can be transmitted with minimum delay. We assume all time intervals to be discretized, and equal to some integer multiple of an underlying clock duration. The details of slot allocation for messages of various types are discussed in [**?**]. The static, globally known schedule allows the nodes to stay in the low-power model maximally since all receivers need to be awake only during slots when they expect to receive some data. The static schedule can, however, be updated as needed through operation and management (OAM) messages that we do support.

To distinguish regular data transfers from OAM, we call the former regular communications (RC). RC in CDMN typically involves a continuous stream with some fixed interval. This allows the possibility of applying some adaptive filtering to reduce communications energy consumption. For example, if the receiver can easily predict the next sample, it need not be communicated. This can be done by putting a Kalman filter-based closed-loop prediction mechanism that we have designed and tested. Essentially, the idea is that the sender keeps track of the change in signal from the last sent value, say ϵ, and the ϵ is adjusted dynamically based on the signal prediction error computed by the receiver. This mechanism does require feedback from the receiver to the sender, which can be less frequent than the signal communication itself [**?**].

To handle such control messaging, we introduce another type of communication, henceforth called keep-alive (KA). The most basic function of KA messages is to alert the receiver of a problem with the sender's functionality. However, instead of making it a distinct keep-alive message, we also use it for regular data transfer (if relevant) and for sending OAM messages. To avoid unnecessary communications, any regular data transfer within one inter-message interval is skipped, and instead that data is sent as a KA message. We also constrain certain OAM messages (e.g., communication of energy needs) to be bundled with the KA communications. Since all communications in CDMN are very short, many messages can be bundled in one packet. For this, we can associate 3 fields with each message: (a) type, (b) count, and (c) length. Here "count" allows us to accumulate multiple messages of the same type and then send them as a batch.

B. Energy Transfer Issues

Unlike communications, energy transfers do not have any interference problems; however, they do bring in several additional scheduling issues, especially when integrated with communications. The energy transmissions are expected to be rather long (in contrast with very short communications) depending on the energy deficits. Energy transfers can be easily broken up into multiple shorter transfers but they do bring in some pros and cons. Furthermore, while it is beneficial for the communications to simply ride over the (longer) energy transfers whenever possible, this may complicate energy/communications scheduling.

The energy broadcasts from the OBN to all the other network nodes directly. This is in contrast with the data and control communications that go between sensors and hubs, and hubs and OBN. There are 3 aspects to consider in energy transfer: (a) Time between successive energy transmissions, (b) Energy transmission duration, and (c) Set of energy receivers during a transmission.

Fig. 2 shows the interactions between different types of nodes, primarily in the energy transfer context but also indicating communication/energy integration where relevant. The LHS dotted box contains the sensor functionality. It shows that each data sample to be transmitted is also accompanied by the energy level of the node. The RHS dotted box shows the hub functionality. A hub receives data (and energy level) from all its sensors and prepares the data that it would send to the OBN. This may involve a simple batching of data from all sensors, their aggregation, or the computation of some new quantity. In all cases, the hub sends its own energy needs and that of all its nodes to the OBN along with the regular data. If there is no regular data to send to the OBN, the KA communication will ensure that the energy needs are communicated to the OBN eventually. The hub also responds to its sensor nodes, at least at KA intervals, with the new threshold value to regulate data transmissions from sensors.

[1] Implanting high data-rate devices like a camera is not practical because of its energy requirements.

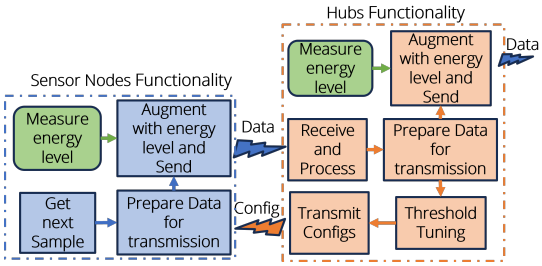

Fig. 2: Sensor node and Hub functionality

In the following, we divide the energy transfer operations into Normal and Low energy states. The *normal state* of the network means that most of the nodes have enough energy to operate all regular tasks. The *low state* of the network is when either the system has too many low-energy nodes, the OBN is low on energy, or the OBN is removed. A temporary removal of OBN (whether a smartwatch or special health-band) is expected; for example, to charge it or take a shower. We do need to put a limit on the total amount of off time as discussed later.[2]

In the following, we describe two energy transfer strategies, Centralized and decentralized. The energy level of each node (%) is classified into three statuses: **High**, **Low**, and **Very Low**. These are characterized by two thresholds, VLT (Very Low Threshold), which separates Very Low from Low, and HT (High Threshold), which separates Low from High.

C. Centralized Energy Transfer Strategy

The objective of the centralized strategy is to select a subset of nodes (guests) to harvest (or receive) energy at designated times. Each node in the network (sensors and hubs) periodically reports its energy level to the OBN. The OBN decision-making process splits its functionality into two key components:

- The *predictor* estimates the future energy levels of each node and sends these estimates to the decision-maker.
- The *decision-maker* selects a set of nodes for energy replenishment based on these predictions, aiming to maximize energy efficiency across the network.

The diagram in Fig. 4 illustrates the interactions between the OBN and the nodes in the centralized strategy. On the left side, we show the OBN's role, which includes storing data, preparing for energy transfers, determining the receivers/guests (either by solving the optimization problem, or sending the data to an outside computer and receiving the solution), and initiating the transfer process. On the right side, the energy reception process at the node level is shown, detailing how nodes prepare to receive and process the invitation, and based on that, start or stop harvesting.

We define the sets of nodes with **very low** and **low** energy levels at time t as S_t^{vlow} and S_t^{low}, respectively. At each energy transfer event, indexed by k, the centralized strategy selects a set of nodes, s_k^{recv}, to receive energy, and the size of the selected set $|s_0^{recv}|$ is predefined. The goal is to find the set $s_k^{recv} \in S_k$ (for kth energy transfer) that maximizes the following utility function for each energy transfer event:

$$U_k = \left(\sum_{i=1}^{|s_0^{recv}|} (\text{sort}(E_{t_s}(s_k^{recv})))_i - \gamma \frac{|S_{t_s}^{low}|}{N} * 100 \right) \quad (1)$$

where:

- t_s indicate the point in time just before the $k+1$th energy transfer. (We omit $k+1$ from these to avoid clutter).
- $\sum_{i=1}^{|s_k^{recv}|}(\text{sort}(E_{t_s}(s_k^{recv})))$ is the summation of the first $|s_k^{recv}|$ minimum energy nodes after the energy transfer to the nodes in the set s_k^{recv}.
- γ is a regularization parameter that penalizes the presence of low-energy nodes.
- $|S_{t_f}^{low}|/N * 100$ is the percentage of nodes that are in the low-energy state at the end of energy transfer.

As a subset of very low- and low-energy nodes that ought to get energy, we define S_k, excluding high-energy nodes. The binomial coefficient counts the possible selections for S_k, based on choosing $|s_0^{recv}|$ nodes from $|S_{t_s}^{vlow} \cup S_{t_s}^{low}|$.

The gain term is defined as the sum of energy levels from the s_0^{recv} lowest-energy nodes. We selected this approach after examining both system-wide mean energy and minimum node energy metrics. Using only the mean energy resulted in the sacrifice of certain nodes to maintain a high average, while focusing solely on the minimum energy level neglected the broader energy distribution. Our partial mean approach strikes a balance: monitoring the most vulnerable nodes while ensuring adequate energy levels across a minimum threshold of nodes.

We incorporated regularization to encourage the system to address critically low-energy nodes promptly. However, this mechanism could produce an adversarial effect, causing the system to prioritize nodes approaching the danger threshold at the expense of nodes already at the lowest energy levels. This trade-off requires careful calibration to ensure optimal energy distribution across the network.

Since CDMNs will typically be very small, we can evaluate all of $O(N \cdot |S_k|)$ possible combinations of nodes in S_k. For each combination s_k^{recv}, the energy mapping function $E_{t_f}(s_k^{recv})$ updates the energy levels after the transfer, ensuring that each node in s_k^{recv} receives energy according to its path-loss. For larger networks, we can instead use a greedy search that iteratively builds s_k^{recv} initially from an empty set, selecting nodes with energy below HT to optimize the utility U_k. At each step, it evaluates replacing the current set with each eligible node (lower energy level), simulates post-transfer energy E_{t_s} considering MRC path loss, and adds the node maximizing utility until $|s_k^{recv}| = |s_0^{recv}|$. Such an approach has polynomial complexity of $O(N \cdot |s_0^{recv}|^2)$.

The default optimization style is full optimization, where the problem is solved anew each time. A potential problem with full optimization is that the solution (set of nodes to be fed energy) may change each time. An alternative is incremental optimization, where we do the full optimization infrequently and largely determine the best incremental update to the last solution. It appeared at first that full optimization was responsi-

[2]While the OBN is off, a permanent on-body backup node may be needed to support basic medical alerting, but we do not consider that aspect here.

ble for the centralized algorithm failing in some cases because it selected a different set of nodes to feed each time. However, the incremental method also has a problem – retaining some nodes in the set meant that some nodes might receive more energy than needed at the expense of others, thereby leading to failure under low energy availability scenarios.

The Greedy Centralized energy transfer process is summarized in Alg. I. In each energy transfer period, the algorithm needs to run once. The execution of the algorithm can happen outside of OBN, but the delay induced in such a scenario should be considered and included in the schedule of energy transfer. Both strategies require an efficient energy level measurement, which can be done by monitoring the voltage change across the capacitor.

Alg. I: Greedy Centralized Energy Transfer Strategy Energy

Input: E := Energy levels; VLT := Very Low threshold; HT := High threshold; $|s_0^{recv}|$:= Target set size; γ := penalty parameter; s_{k-1}^{recv} := previous round's selected set
Output: s_k^{recv} := Updated set for energy transfer in round k
Variables: S := Eligible nodes ($E_i \leq HT$); U_k := Utility; U_{max} := Max utility; S^{best} := Best set
Algorithm:
Initialize $S \leftarrow \{i \mid 0 < E_i \leq HT\}$
$S^{best} \leftarrow s_{k-1}^{recv}$, Simulate $E_{t_s}(S^{best})$; compute U_{max}, $improved \leftarrow$ True
While $improved$ {
  $improved \leftarrow$ False
  Simulate $E_{t_s}(S^{best})$ and sort by energy descending
  For each $i \in S \setminus S^{best}$ {
    Simulate $E_{t_s}(i)$
    For each $j \in S^{best}$ with $E_{t_s}(j) > E_{t_s}(i)$ {
      $candidate \leftarrow (S^{best} \setminus \{j\}) \cup \{i\}$
      Simulate and sort $E = E_{t_s}(candidate)$
      Compute $U_k = \left(\sum_{\ell=1}^{|s_0^{recv}|} \mathrm{E}[\ell] - \gamma \cdot \frac{|S_{tf}^{low}|}{|E|} \cdot 100 \right)$
      If $U_k > U_{max}$ **then** {
        $S^{best} \leftarrow candidate$, $U_{max} \leftarrow U_k$, $improved \leftarrow$ True
}}}}}
Return $s_k^{recv} \leftarrow S^{best}$

D. Decentralized Energy Transfer Strategy

The objective of the decentralized strategy is to allow nodes to make autonomous decisions during energy transfers without waiting for specific invitations from the OBN. The role of the OBN is limited to initiating the kth energy transfer. Once the transfer begins, each node independently evaluates its energy level and decides whether or not to participate in the energy harvesting process.

For a node j, the probability of harvesting energy, P_H, is defined by the following probability function:

$$P_H(j) = \begin{cases} 0 & \text{if energy status is High,} \\ \left(\frac{HT - E(j)}{HT - VLT}\right)^{\alpha} & \text{if energy status is Low,} \\ 1 & \text{if energy status is Very Low.} \end{cases} \quad (2)$$

Here, α is a positive configuration parameter, which is uniquely defined for each node, that adjusts the harvesting probability profile, e.g. higher α corresponds to a lower chance of harvesting for a node. Right before each energy transfer, each node calculates its energy status and then computes the probability of harvesting based on this function during each energy transfer. We also add a back-off mechanism, to account for consecutive failures in harvesting attempts. Each node keeps a failure counter, and if a node attempts to harvest energy but fails, the counter increments, otherwise, it resets to 0. If a failure counter of a node reaches C, the system adjusts the harvesting probability $P_H(j)$ to 1, ensuring that the node will successfully harvest energy during the energy transfer. After that, the failure counter resets to 0 and the usual process is used in the next transfer.

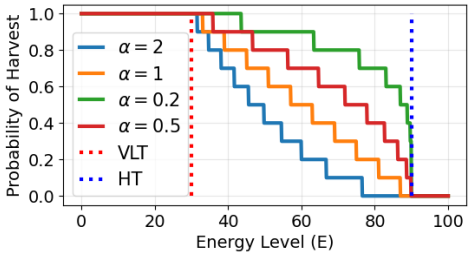

Fig. 3: Probability of Harvesting

Alg. II: Decentralized Energy Transfer Pseudocode

Input: E := Energy level of node j at time k
Parameters: VLT := Very Low Threshold; HT := High Threshold; α := Probability exponent; C := Failure Threshold
Output: Decision for node j to participate in energy harvesting
Variables: $FailCount(j)$:= Failure counter for node j; P_H := Harvesting probability
Algorithm:
Compute $status \leftarrow Status(E(j), VLT, HT)$
If $status$ is Very Low || $FailCount(j) = C$ **Then** $P_H \leftarrow 1$
Else If $status$ is High **Then** $P_H \leftarrow 0$
Else If $status$ is Low & $FailCount(j) < C$ {
  $P_H \leftarrow (\frac{HT - E(j)}{HT - VLT})^{\alpha}$
  Sample $Result \sim Binom(P_H)$
  If $Result$ is failed **Then** $FailCount(j) \leftarrow FailCount(j) + 1$
  Else $FailCount(j) \leftarrow 0$
}

The decentralized energy transfer process is summarized in Alg. II. Each node makes an independent decision on whether to participate in harvesting based on its current energy status and probability calculations. Note that the calculation of $(\frac{HT - E(j)}{HT - VLT})^{\alpha}$ is expensive, but one could easily precompute and load it into a table for online use. Fig. 3 illustrates the probability of harvesting against energy level along with discretization in steps 10% probability.[3]

The diagram in Fig. 4 illustrates the interactions between the OBN and the nodes in the decentralized strategy (yellow path). On the left side, we show the OBN's limited role, which includes storing data, preparing for energy transfers, and initiating the transfer process. On the right side, the energy reception process at the node level is shown, detailing how nodes measure their energy levels, classify themselves into the appropriate energy status, and independently decide whether to harvest energy based on the decentralized strategy algorithm.

[3]The discretization here is only for illustration; it could use larger or smaller steps without much impact.

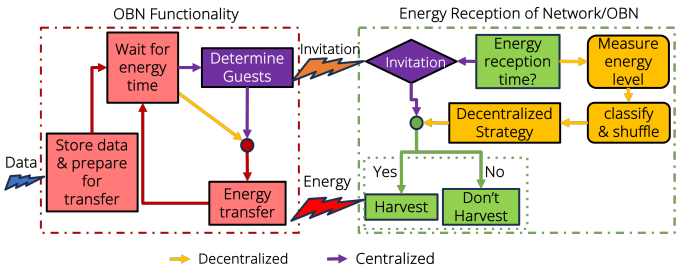

Fig. 4: Centralized and Decentralized Strategies

E. Scalability

The centralized strategy relies on accurate energy approximations, but poor estimates can lead to mismanagement of low-energy nodes. In contrast, the decentralized approach allows nodes to make real-time, independent decisions, offering greater flexibility. However, the decentralized approach suffers from higher path loss as more nodes independently harvest energy. While this can be considered as a scalability limitation, practical CDMNs are typically very small, as already stated. However, if we do want to design large intra-body networks, a single OBN will be inadequate; instead, we should divide them into clusters, each powered by a separate OBN, preferably located close to the cluster.

F. Energy Transfer Scheduling

1) Global Schedule: We consider a common global schedule for all the nodes communications and energy transfer in the network (detailed explanation is provided in [**?**]).

2) Energy Level Prediction: The energy consumption of each node can be divided into nominal energy expenditure (e.g., leakage, sampling, computations), and communications, which depends on the number of communications. Since the nominal energy expenditure remains the same, the only variable that needs to be tracked to predict the energy level is the number of communications. It can be shown that the number of communications of each node, is bounded from above and below by RC and KA signal periods. The task is then to track the number of transmissions and receptions by each node. Since the main objective is to have an energy-efficient system, the method implemented should be fairly simple (to minimize the lag between receiving the energy level data) and accurate. Depending upon the cost of each communication, the importance of accuracy can be high or low, e.g., the more expensive the communication is, the greater contribution it has on the overall energy expenditure, and hence the accuracy can be a critical objective.

IV. Experimental Evaluation

Given the context of an intrabody network, a direct evaluation is largely infeasible; therefore, our approach is to characterize the communication media of the body via actual experiments and then build a comprehensive simulation model that represents various aspects of communication and energy transfer. Unfortunately, there are no small commercial MRC devices that would be suitable even for on-body use, therefore, much of our data concerning MRC through the human body comes from two types of experiments done using custom-built antennas: (a) Signal propagation experiments, and (b) Packet transfer experiments facilitated by connecting antennas on each end with USRP boards that support packet formation, modulation/demodulation, and received packet processing. While these experiments provide a good channel characterization, the calibration of energy-related parameters is largely based on available data from short-range and body area network (BAN) experiments or products in the literature.

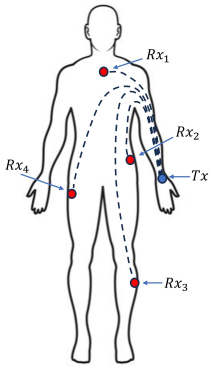

Fig. 5: MR receiver placements

A. On-Body Experiments for Channel Characterization

From an energy delivery perspective, we need to study the impact of multiple simultaneous MRC receivers, which has not been addressed by prior work on MRC. For this, we conducted an experiment with a single transmitter MRC coil on the wrist and multiple receiver coils on the chest, waist, hip, and calf (see Fig. 5). The experimental setup is the same as in [26]. The average through-the-body distances between the transmitter (T_x) and receivers (R_x) were approximately 60 cm, 100 cm, 160 cm, and 130 cm, respectively.

In a four-receiver system, 15 unique configurations arise when one or more receivers are activated simultaneously. Since the transmitted power is fixed, increasing the number of active receivers reduces the power received per receiver. Table III lists the average path loss for configurations with varying numbers of receivers.

Number of Receivers	Average Path Loss (dB)
1 receiver	-18.80
2 receivers	-20.63
3 receivers	-22.56
4 receivers	-23.80

Alg. III: Average Path Loss for with Multiple Receivers

Simulations used artificial path-loss lists to model power-sharing behavior. Two clusters were created: Cluster 1 (one hub and three sensors) and Cluster 2 (one hub and two sensors). Cluster 1 starts with a path-loss of -19 dB, while Cluster 2 starts at -20 dB:

$$\begin{aligned} \text{Cluster 1 PL} &= \{-19, -20, \ldots, -25\}, \\ \text{Cluster 2 PL} &= \{-20, -21, \ldots, -26\}. \end{aligned} \tag{3}$$

In this setup, the index represents the number of participating nodes. For example, with three receivers (two from Cluster 1 and one from Cluster 2), path-loss values are -20 dB for Cluster 1 and -22 dB for Cluster 2.

B. Simulated CDMN Characteristics

We assume an intrabody network of 7 nodes (5 sensor nodes and 2 hub nodes). We divide the nodes into 2 clusters, one of which is closer to the OBN (hence the lower path-loss). The

OBN is a smartwatch with a battery capacity of 500mAh and an operating voltage of 3.6V. We assume the normal usage of 40mW and 1mW of losses related to the energy transfer circuit. We introduce a tiered energy transfer scheme on OBN by introducing a multiplier on the base energy transfer: when OBN has above 60% energy, the power transfer is $1.5 \cdot 12mW$, between 30% to 60% it transfers $1.25 \cdot 12mW$, and below 30% it sends $12mW$, resulting in an average of $15.5mW$ until the OBN battery is under 10%. Nominally, we assume that when the OBN battery goes under 10%, it is charged for a maximum of 4 hours, and during that time, it does not do any energy transfer to CDMN. After charging, the OBN restarts energy transfer with a 100% charge.

At each step, the energy provided by OBN can be harvested by $0 < k \leq n$ nodes, with roughly a 1 db loss for each additional node added. Given the $\sim$20db or more signal attenuation, the received energy is in the range of only a few μJ.

We assume regular communication for four sensors is every 30 seconds. Every 2 skipped regular communications results in a mandatory communication on the next slot, i.e., mandatory communication happens every 90 seconds for the first four sensors (minimum and maximum number of communications are 30 and 120). Sensor 5 sends its data every 5 minutes without suppressing any of its communications. Using such a suppression method, the number of communications for sensors 1 to 4 would be limited to 30-120 every hour.

Each node is equipped with a 0.5 F CAP-X supercapacitor [31] operating at 2.7V, providing a total energy capacity of 1.82J. To minimize energy consumption, each node utilizes Microchip's XLP MCU [32]. The specifications of both components are summarized in Table IV.

Component	Cost			
	Capacity(F)	Leakage(μA)	Voltage(V)	ESR(Ω)
Capacitor	0.5	1	2.7	0.57
	Voltage(V)	Active(μA)	Idle(μA)	Sleep(μA)
MCU	1.8-3.6	155	50	0.2

Alg. IV: Component Specifications

Although publicly available physiological signals such as heart rate can be used to evaluate the impact of energy delivery algorithms, an artificial signal provides much greater control for stress testing. Accordingly, we used a combination of real and artificial signals in our evaluation. In particular, for the first four sensors, we extracted the number of communications obtained from our Kalman Filter-based closed-loop control [**?**] that used the BVP and IBI from the dataset in [33]. Sensor 5 used the glucose level data from the same dataset. The simulation ran for 10 hours, and from the sensor to the hub, we achieved 52, 42, 65, and 75 signals per hour on average with standard deviations of 11, 6, 8, and 8, respectively.

Out of the data from sensors 1 to 4, we created a sinusoidal signal with DC shift and random frequency modulation to represent the pseudo-periodic physiological signals like BVP. We adopted this model to construct a pseudo-periodic signal that captures the rhythmic essence of physiological data, while offering precise control over frequency and amplitude. This approach enables effective stress testing of our energy delivery algorithms under tailored, representative conditions. Each signal had an amplitude of its standard deviation times $\sqrt{2}$ (to remove the standard deviation of the sine wave) and a DC shift equal to the obtained average of each signal, consistent with the signals that we analyzed. At each sampling instance, the frequency f was randomly drawn from a uniform distribution $[10, 50]$, and the signal was computed as:

$$S(t) = \sigma\sqrt{2} \cdot \sin(2\pi f t) + \text{dc\_shift}, \tag{4}$$

where $S(t)$ is the signal value at time t, and the dc_shift is sensor-specific. Communication counts are sampled directly from these signals, incorporating frequency variability and sensor-specific characteristics. We assume the same energy cost for reception and transmission. The hub-to-sensor transmissions, which include threshold updates and configurations, are much fewer and are simulated to be one-half of the maximum number of communications from supervised sensors to their supervising hub. In most cases, the hub-to-sensor communication is likely to be less frequent, one-half represents a somewhat extreme situation.

We implemented an ARIMA (AutoRegressive Integrated Moving Average) model to predict future energy consumption values for each node based on historical data. Specifically, the model was configured to capture linear autoregressive behavior and account for potential non-stationarity through first-order differencing. The forecasting process dynamically updates predictions at each time step, ensuring adaptability to real-time variations in energy usage patterns. To align predictions with operational constraints, the forecasted values are clipped to a predefined range of 30 to 120, reflecting the practical limits of the data range in our system. This approach allows for robust and computationally efficient energy trajectory evaluation across all nodes, facilitating effective resource management and communication scheduling in distributed sensor networks.

In terms of energy, the code monitoring shows about 300 instructions (worst case) for the Kalman filter at the hubs, and the number of instructions for running the centralized strategy is 264 instructions, which is done by the OBN. Clearly, the energy expense of the decentralized algorithm is much smaller (at worst, 30 instructions). The energy consumption values for sensing, transmission, and reception are listed in Table V.

Type	Cost	Duration
Transmission/Reception	350μW	5ms
Sensors 1 to 4	75μW	10ms
Sensor 5	1.87μW	1000ms

Alg. V: Energy Consumption in an hour

C. Centralized vs. Decentralized Energy Transfers

We explore energy transfer effectiveness of centralized and decentralized mechanisms under two scenarios: (1) **Charge-on-low** where the OBN is used for 20 hours during the day, then removed for 4 hours of charging, and put back again, and

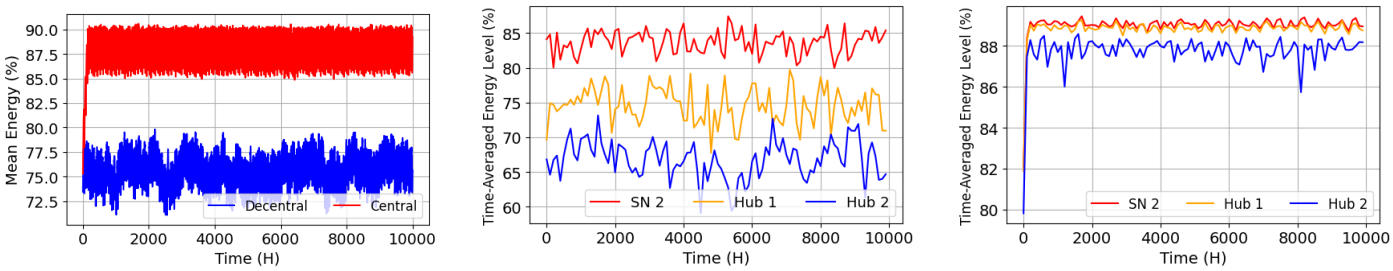

Fig. 6: **Charge-on-low**: (a) Mean Energy Trajectory, (b) Decentralized Strategy, (c) Centralized Strategy

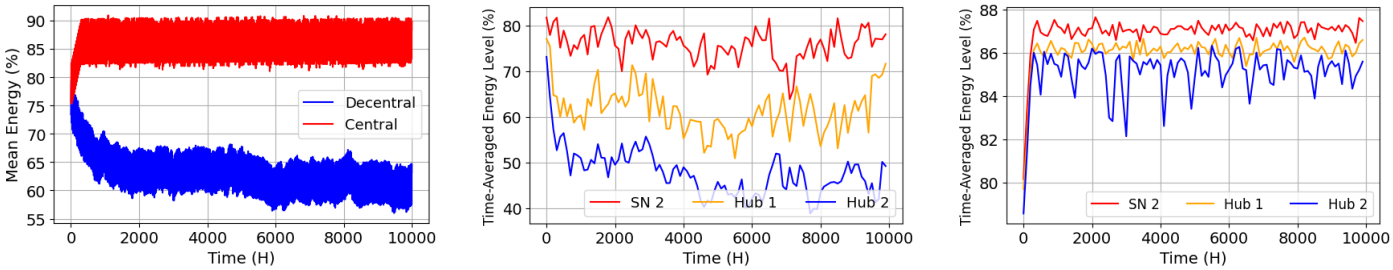

Fig. 7: **Regular-charging with increased energy**: (a) Mean Energy, (b) Decentralized Strategy, (c) Centralized Strategy

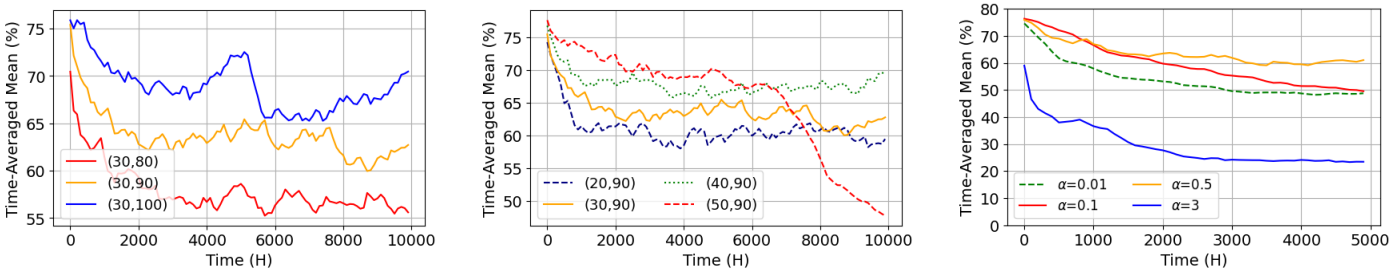

Fig. 8: (a) Effect of VLT, (b) Effect of HT (c) Effect of different αs

(2) **Regular-charging** where the OBN is taken off and left to charge for 10 hours each night and then put back.

Note that in the regular-charging scenario, the CDMN nodes receive energy only for 14 hours out of 24, as opposed to 20 hours in the charge-on-low case. Thus, for a fair comparison, we increase the energy transfer amount for the second case by 20/14 = 1.43 times.

In terms of difficulty, Charge-on-low is an easier scenario than the Regular-charging scenario. The figures in this section show the simulated energy transfer behavior over 5000 or 10000 hours of operation. As a default, the centralized strategy provides energy to 4 receivers, and for the decentralized strategy α is set to 0.5 for all the nodes, and VLT and HT are set to 30% to 90% for both strategies. The regularization parameter γ is set to 1 by trial and error. To make the trajectories clearer, we use a time-average mean calculation, where the mean over all the nodes is averaged over 100 hours for the whole simulation time.

In the Charge-on-low case, Figs. 6(a) shows the mean energy of all nodes (as a percentage of their full capacity). Figs. 6(b) and (c) provide further detail – energy of 3 representative nodes (Sensor Node 2 (SN2) lowest, Hub1 medium, Hub2 highest) for decentralized and centralized strategies, respectively. Figs. 7(a)-(c) show these quantities for regular charging. It is seen that the 10 hour charging gap per day causes higher variations in energy, but the nodes are able to maintain the charge.

The main disadvantage of the centralized strategy is that it prespecifies the number of nodes that can receive energy. Thus, when the energy availability is low, the wrong set of nodes may be fed, thereby leading to failure. The decentralized strategy does not suffer from such behavior, since each node autonomously decides if it wants to harvest. We observed the effect of such behavior in a Regular-charging scenario.

1) Decentralized Scheme with Different Energy Thresholds: The Decentralized Strategy was tested for different values of energy reception thresholds VLT and HT, and the results are shown in Figs. 8(a) and 8(b). In all the cases, α was set to 0.5. Both lower HT and VLT result in lower after convergence values, since in the former, the nodes get satisfied quickly, and in the latter, the probability profile gets stretched, and reaching higher values gets more difficult.

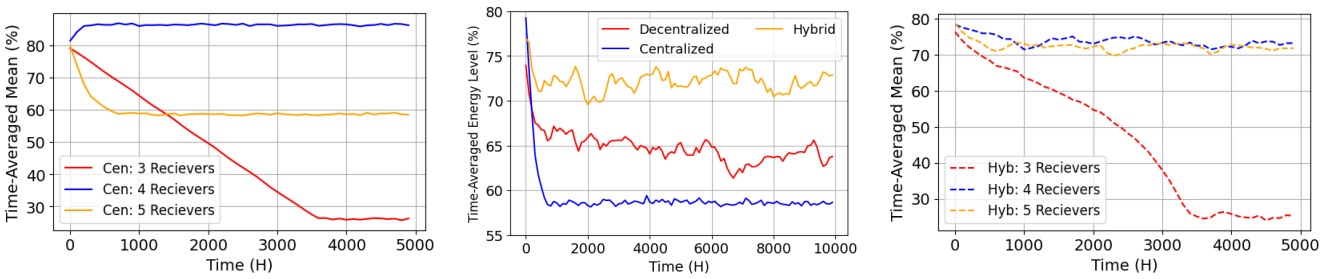

Fig. 9: (a) Effect of number of receivers on CS, (b) Mean Energy Trajectory of Hybrid strategy, (c) Effect of number of receivers on Hybrid strategy

It is clear that a higher HT/VLT results in a higher after-convergence value. However, they are also introducing a hazardous situation where most of the nodes are in very low status, hence all would want to harvest the energy with a probability of 1 (This situation should always be considered and avoided). Both high HT and VLT mean that more nodes would want to harvest the energy: high HT results in more hunger in nodes even with relatively high energy and high VLT means the nodes could get into very low status faster (see how VLT$=50\%$ fails). Both cases are equally bad since they introduce a higher chance of less efficient energy transfer.

The default case (VLT$=30\%$, HT$=90\%$) is stable and offers the third-best post-convergence value, after scenarios HT$=100$ and VLT$=40$. All the other cases considered were either unstable and had very low status nodes, or resulted in less post-convergence value.

2) Impact of α on Decentralized Algorithm: This concerns using the same α value for all the nodes in the network. A lower α means that all nodes have a higher chance of receiving the energy. The results for four different α values are shown in Fig. 8(c). Only $\alpha = 0.5$ is successful in managing and maintaining a value after convergence. Using other values, the nodes lose energy and do not receive enough to compensate for their losses. The only reason the mean energy is still high in both $\alpha = 0.01$ and $\alpha = 0.1$ is that they can push some of their nodes to HT, at the expense of losing the others. By the end of the simulation, $\alpha = 0.01$ had 3 nodes, $\alpha = 0.1$ had 2 nodes, and $\alpha = 3$ had 6 nodes in the low state.

It should be noted that introducing a higher α would reduce the mean energy since there is a smaller chance of reaching the HT. This suggests that a lower α is better, but it also implies that many nodes would simultaneously want to receive power, thereby increasing the path loss for everyone.

3) Impact of Receive Set Size on Centralized Algorithm: The Centralized Strategy was tested for $|s_0^{recv}|$ (receive set size) of 3, 4, and 5, and the results are shown in Fig. 9(a). As it can be seen, using 3 receivers results in a steady drop, A set size of 3 fails because it cannot transfer energy to enough receivers per period to sustain all nodes, given the energy demands and path loss. Using 5 receivers also does not work properly, as the energy drops drastically until 2 of the receivers are out of energy, and the system would not be able to recover them. This occurs because activating too many receivers increases path loss, reducing energy transfer efficiency. Only using 4 receivers can properly perform the task.

D. Combining Centralized and Decentralized Schemes

In addition to a pure centralized or decentralized mechanism, it is possible to use a combination of the two as well. In this section, we briefly consider a hybrid mechanism that works as follows: Below the mean energy of 50%, we use a decentralized strategy due to its robustness, and above we switch between centralized and decentralized equally to take advantage of the higher mean energy of the centralized scheme without its downside. Fig. 9(b) shows the mean energy with $|s_k^{recv}| = 5$. The hybrid strategy achieves the highest after-convergence value without having any nodes with low energy. Fig. 9(c) shows this scheme also has less sensitivity to the hyperparameter $|s_k^{recv}|$ (of the centralized part). While the fully centralized strategy was stable only for 4 receivers, this one is stable for both 4 and 5 receivers (no low-status nodes).

Simulation results demonstrate that the hybrid outperforms greedy, and hybrid methods in terms of sensitivity and long-run average energy levels. This advantage likely stems from its ability to incorporate controlled stochasticity in the node selection process. While deterministic strategies like the greedy methods tend to follow rigid selection patterns that struggle to adapt to fluctuations in energy consumption, stochastic strategies, such as the hybrid approaches, introduce variability that allows for exploratory decisions. This flexibility enables the system to better respond to dynamic changes, ultimately leading to improved overall performance. It should be mentioned that there could be other variants of the hybrid model, based on the centralized and decentralized strategies.

V. Conclusions

In this paper, we explored the energy delivery strategies to the intra-body chronic disease management networks via an on-body node (OBN) using magnetic resonance communications (MRC). Such energy transfer allows the implanted nodes to operate with a small supercapacitor rather than batteries that are usually big and may need to be replaced. The mechanism accounts for the reduction in received energy when there are multiple receivers. We analyze centralized, fully distributed, and combined (hybrid) energy strategies and show that the last

one works the best. In the future we will study the mechanisms for (1) using biomechanical energy harvested at promising spots in the body (e.g., heart and lungs) to augment the OBN supplied energy to implanted nodes, and (2) using an auxiliary long battery-life OBN in form of stomach patch to support emergency reporting and emergency energy supply when the OBN is taken off for charging.

REFERENCES

[1] W. H. Organization, "World report on aging," https://iris.who.int/bitstream/handle/10665/186463/9789240694811_eng.pdf, 2015.

[2] G. Yang, L. Xie, M. Mäntysalo, X. Zhou, Z. Pang, L. Da Xu, S. Kao-Walter, Q. Chen, and L.-R. Zheng, "A health-iot platform based on the integration of intelligent packaging, unobtrusive bio-sensor, and intelligent medicine box," *IEEE transactions on industrial informatics*, vol. 10, no. 4, pp. 2180–2191, 2014.

[3] L. P. Fried, "America's health and health care depend on preventing chronic disease," https://www.huffingtonpost.com/entry/americas-health-and-healthcare-depends-on-preventing_us_58c0649de4b070e55af9eade, March 2017.

[4] P. Trotter, F. Lobelo, and A. Heather, "Chronic disease is healthcare's rising risk," https://www.healthitoutcomes.com/doc/chronic-disease-is-healthcare-s-rising-risk-0001, June 2017.

[5] A. Tinker, "How to improve patient outcomes for chronic diseases and comorbidities," http://www.healthcatalyst.com/wp-content/uploads/2014/04/How-to-Improve-Patient-Outcomes.pdf, 2017.

[6] C. Powell, "Conditional electrical stimulation in animal and human models for neurogenic bladder: working toward a neuroprosthesis," *Current bladder dysfunction reports*, vol. 11, no. 4, pp. 379–385, 2016.

[7] T. M. Bruns, N. Bhadra, and K. J. Gustafson, "Bursting stimulation of proximal urethral afferents improves bladder pressures and voiding," *Journal of neural engineering*, vol. 6, no. 6, p. 066006, 2009.

[8] A. Mendez, M. Sawan, T. Minagawa, and J.-J. Wyndaele, "Estimation of bladder volume from afferent neural activity," *IEEE Transactions on Neural Systems and Rehabilitation Engineering*, vol. 21, no. 5, pp. 704–715, 2013.

[9] S.-Y. Lee and C.-Y. Huang, "Bladder control implants," in *Handbook of Biochips: Integrated Circuits and Systems for Biology and Medicine*. Springer, 2022, pp. 3–20.

[10] R. G. HAUSER, "Techniques for improving cardiac performance with implantable devices," *Pacing and Clinical Electrophysiology*, vol. 7, no. 6, pp. 1234–1239, 1984.

[11] K. Kaszala and K. A. Ellenbogen, "Device sensing: sensors and algorithms for pacemakers and implantable cardioverter defibrillators," *Circulation*, vol. 122, no. 13, pp. 1328–1340, 2010.

[12] C. Saha, T. O'Donnell, N. Wang, and P. McCloskey, "Electromagnetic generator for harvesting energy from human motion," *Sensors and Actuators A: Physical*, vol. 147, no. 1, pp. 248–253, Sep. 2008. [Online]. Available: https://linkinghub.elsevier.com/retrieve/pii/S0924424708001398

[13] K. Li, Q. He, J. Wang, Z. Zhou, and X. Li, "Wearable energy harvesters generating electricity from low-frequency human limb movement," *Microsystems & nanoengineering*, vol. 4, no. 1, pp. 1–13, 2018.

[14] P. Pandit, H. Kia, and K. Kant, "Integrated communications and energy management in intra-body networks," April 2025, submitted for publication, Available at https://www.kkant.net/papers/Integrated_comm_paper.pdf.

[15] B. L. Cannon, J. F. Hoburg, D. D. Stancil, and S. C. Goldstein, "Magnetic resonant coupling as a potential means for wireless power transfer to multiple small receivers," *IEEE transactions on power electronics*, vol. 24, no. 7, pp. 1819–1825, 2009.

[16] K. Zhang, C. Liu, Z. H. Jiang, Y. Zhang, X. Liu, H. Guo, and X. Yang, "Near-field wireless power transfer to deep-tissue implants for biomedical applications," *IEEE Transactions on Antennas and Propagation*, vol. 68, no. 2, pp. 1098–1106, 2019.

[17] Ting Chia Chang, M. Weber, J. Charthad, A. Nikoozadeh, P. T. Khuri-Yakub, and A. Arbabian, "Design of high-efficiency miniaturized ultrasonic receivers for powering medical implants with reconfigurable power levels," in *2015 IEEE International Ultrasonics Symposium (IUS)*. Taipei, Taiwan: IEEE, Oct. 2015, pp. 1–4. [Online]. Available: http://ieeexplore.ieee.org/document/7329613/

[18] S. R. Khan, S. K. Pavuluri, G. Cummins, and M. P. Y. Desmulliez, "Wireless Power Transfer Techniques for Implantable Medical Devices: A Review," *Sensors*, vol. 20, no. 12, p. 3487, jun 2020. [Online]. Available: https://www.mdpi.com/1424-8220/20/12/3487

[19] J. Van Mulders, D. Delabie, C. Lecluyse, C. Buyle, G. Callebaut, L. Van der Perre, and L. De Strycker, "Wireless power transfer: Systems, circuits, standards, and use cases," *Sensors*, vol. 22, no. 15, p. 5573, 2022.

[20] Y. Lim, H. Tang, S. Lim, and J. Park, "An adaptive impedance-matching network based on a novel capacitor matrix for wireless power transfer," *IEEE Transactions on Power Electronics*, vol. 29, no. 8, pp. 4403–4413, 2013.

[21] K. Song, G. Yang, H. Zhang, X. Huang, J. Jiang, Y. Lan, X. Huang, J. Li, and C. Zhu, "An impedance decoupling-based tuning scheme for wireless power transfer system under dual-side capacitance drift," *IEEE Transactions on Power Electronics*, vol. 36, no. 7, pp. 7526–7536, 2020.

[22] A. Ali, H. Shaukat, S. Bibi, W. A. Altabey, M. Noori, and S. A. Kouritem, "Recent progress in energy harvesting systems for wearable technology," *Energy Strategy Reviews*, vol. 49, p. 101124, 2023.

[23] M. Mariello, "Heart energy harvesting and cardiac bioelectronics: technologies and perspectives," *Nanoenergy Advances*, vol. 2, no. 4, pp. 344–385, 2022.

[24] K. R. S. Kumar and S. Gopikrishnan, "Caddisfalcon optimization algorithm for on-demand energy transfer in wireless rechargeable sensors based iot networks," *Sustainable Energy Technologies and Assessments*, vol. 64, p. 103732, 2024.

[25] F. Meng, P. Chen, L. Wu, and J. Cheng, "Power allocation in multi-user cellular networks: Deep reinforcement learning approaches," *IEEE Transactions on Wireless Communications*, vol. 19, no. 10, pp. 6255–6267, 2020.

[26] H. Kia, R. Gulati, and K. Kant, "A study of magnetic resonance and ultrasound based through-the-body communications," *Proc. of IEEE WiMob conference*, Oct 2024.

[27] H. Kia and K. Kant, "Autotuning of resonant magnetic induction communications," *Accepted for DCOSS-IoT (Intl. conf. on dist. computing in Smart Systems and IoT), available at https://www.kkant.net/papers/qfactor_tuning.pdf*, April 2024.

[28] R. K. Gulati, S. Islam, A. Pal, K. Kant, and A. Kim, "Characterization of magnetic communication through human body," *IEEE Consumer Communications and Networking Conference (CCNC)*, pp. 563–568, Jan 2022.

[29] S. Islam, R. K. Gulati, M. Domic, A. Pal, K. Kant, and A. Kim, "Performance evaluation of magnetic resonance coupling method for intra-body network (ibnet)," *IEEE Transactions on Biomedical Engineering*, vol. 69, no. 6, pp. 1901–1908, June 2022.

[30] A. Pal and K. Kant, "Magloc: A magnetic induction basedcommunication scheme for fresh food logistics," *Elsevier IoT Journal*, vol. 19, Aug 2022.

[31] CAP-XX, "Cap-xx gy series supercapacitor datasheet (v4.5)," February 2024. [Online]. Available: https://www.cap-xx.com/wp-content/uploads/2024/02/CAP-XX-GY-series-Datasheet-V4_5.pdf

[32] Microchip Technology Inc., "extreme low power (xlp) pic® microcontrollers," 2023. [Online]. Available: https://ww1.microchip.com/downloads/en/DeviceDoc/30009941J.pdf

[33] P. Cho, J. Kim, B. Bent, and J. Dunn, "Big ideas lab glycemic variability and wearable device data," *(version 1.1.1). PhysioNet*, 2023.